JACS
JOURNAL OF THE AMERICAN CHEMICAL SOCIETY
Article
pubs.acs.org/JACS

Monolayered Nanodots of Transition Metal Oxides

Keisuke Nakamura, Yuya Oaki,* and Hiroaki Imai*

Department of Applied Chemistry, Faculty of Science and Technology, Keio University, 3-14-1 Hiyoshi, Kohoku-ku, Yokohama 223-8522, Japan

Supporting Information

ABSTRACT: Monolayered nanodots of titanium, tungsten, and manganese oxides were obtained by exfoliation of the nanocrystals through aqueous solution processes at room temperature. The precursor nanocrystals of the layered compounds, such as sodium titanate ($Na_{0.80}Ti_{1.80}\square_{0.2}O_4{\cdot}xH_2O$, $\square$: vacancy ($x < 1.17$)), cesium tungstate ($Cs_4W_{11}O_{35}{\cdot}yH_2O$ ($y < 10.5$)), and sodium manganate ($Na_{0.44}MnO_2{\cdot}zH_2O$ ($z < 0.85$)), were synthesized in an aqueous solution. These nanocrystals of the layered compounds were delaminated into the monolayered nanodots through introduction of a bulky organic cation in the interlayer space. The resultant monolayered nanodots of the titanate and tungstate 2−5 nm in lateral size showed a remarkable blueshift of the bandgap energies. The calculation studies supported the blueshifts of the bandgap energies. The results suggest that syntheses of monolayered nanodots can expand the tuning range of the properties based on size effect. The present approaches for generation of ultrathin tiny objects can be applied to a variety of nanomaterials.

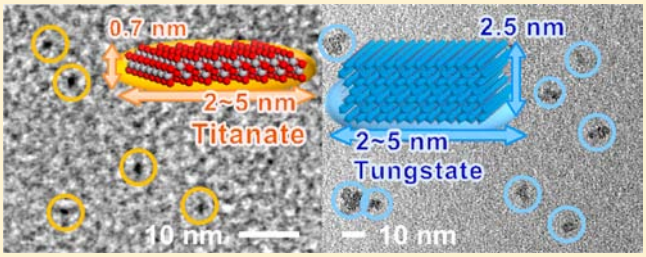

INTRODUCTION

Morphology control of low-dimensional nanostructures has attracted much interest.[1,2] If the thickness of nanodots or the lateral size of monolayered materials is decreased, monolayered nanodots can be obtained as an ultrathin tiny structure. These two schemes for nanoscale morphology control have potentials for tuning of the properties based on size effect. Our intention here is to synthesize monolayered nanodots of transition metal oxides. The monolayered nanodots of three transition metal oxides have been synthesized through solution processes at room temperature: titanium oxide 2−5 nm in size and 0.7 nm in thickness, tungsten oxide 2−5 nm in size and 2.5 nm in thickness, and manganese oxide around 10 nm in size and 0.6 nm in thickness. Nanoparticles with controlled size and their assemblies have been synthesized by a variety of methods.[2−12] A number of monolayered sheets with a lateral size in the micrometer scale, a two-dimensional (2D) nanomaterial, were prepared by delamination of layered inorganic compounds.[13−18] However, exfoliation of nanocrystals and reducing the lateral size of monolayered sheets were not fully studied in previous works.

In semiconductor materials, it is expected that exfoliation of nanocrystals and reducing the size of monolayers lead to a blueshift of the bandgap energy (ΔE_g). The ΔE_g in 2D planar nanostructures is described by the following equation (eq 1):[15e,19]

$$\Delta E_g = \frac{h^2}{4\mu_{xy}L_{xy}^{\ 2}} + \frac{h^2}{8\mu_z L_z^{\ 2}} \quad (1)$$

where x and y are the coordinates parallel to the plane, z is the coordinate perpendicular to the plane, L_i (i = xy, z) is the length of each coordinate, μ_{xy} and μ_z are the reduced effective masses of the electron−hole pair in the corresponding coordinates, and h is Planck's constant. The ΔE_g with formation of the monolayered nanodots is estimated by the eq 1. Figure 1 shows the calculated blueshifts of the bandgap energy with exfoliation of nanostructures with the lateral size in the nanometer scale (curve i in Figure 1) and decreasing the size of monolayers on the assumption of the different μ_{xy} and μ_z values (curves ii−vi in Figure 1). Herein, a titanium oxide compound is adopted as a model. The μ_{xy} value is assumed to be $1.63m_e$ same as that of bulk anatase titanium dioxide.[20] The μ_z value is referred to that of the micrometer-sized titanate monolayers, namely, $1.28m_e$, as reported in a previous paper.[15e] Exfoliation of the layered nanostructures with L_{xy} = 2.0 nm in lateral size can be represented by a decrease in L_z (curve i in Figure 1a). Reducing the lateral size of monolayers can be represented by the decrease in L_{xy} under the constant L_z = 0.7 nm (curve ii in Figure 1a). These two curves represent the variation of ΔE_g with formation of monolayered nanodots. If the monolayered nanodots L_{xy} = 2.0 nm in size and L_z = 0.7 nm in the thickness are formed (the circled and squared plots in Figure 1a), the blueshift of the bandgap energy is calculated to be ΔE_g = 0.71 eV compared to bulk anatase crystal with a bandgap energy (E_g) of 3.2 eV.[21] The blueshift will be the largest value as reported in titanium oxide related materials.[22] If the effective masses are supposed to be the smaller values, the

Received: January 14, 2013
Published: February 27, 2013

dx.doi.org/10.1021/ja400443a | J. Am. Chem. Soc. 2013, 135, 4501−4508

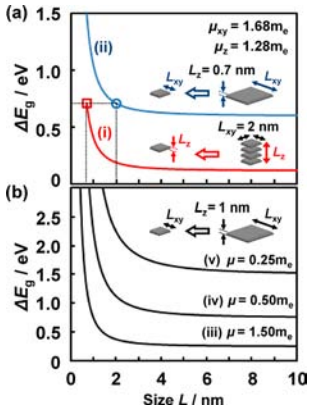

Figure 1. Estimated blueshift of the bandgap energy (ΔE_g) based on eq 1 through the exfoliation of the nanostructures (curve i) and the decreasing of the lateral size of monolayers (curves ii–vi) on the assumption of the different μ_{xy} and μ_z values: (a) a model case of μ_{xy} = $1.68m_e$ and μ_z = $1.28m_e$ on the assumption of the layered titanate compound; (b) the influence of the μ_{xy} and μ_z values on ΔE_g. Curve i represents the exfoliation of the nanostructures with the changes of L_z at the constant L_{xy} = 2 nm. Curve ii represents the reducing of the size of monolayered sheets with the changes of L_{xy} at the constant L_z = 0.7 nm. The plots of a square and a circle represent the formation of the monolayered nanodots. Curves iii–vi show the reducing of the size of monolayered sheets with the changes of L_{xy} on the assumption of the constant L_z = 1 nm. In curves iii–vi, μ is defined as $\mu = \mu_{xy} = \mu_z$ and changed from $1.50m_e$ to $0.25m_e$.

more remarkable blueshift of the bandgap energy can be observed by the formation of the monolayered nanodots (Figure 1b). For example, a monolayered compound with the L_z = 1.0 nm is assumed to study the effect of the μ_{xy} and μ_z values. If the μ_{xy} and μ_z values are decreased from $1.5m_e$ to $0.25m_e$, larger ΔE_g values can be obtained on the same size of the monolayered nanodots. These calculations imply that formation of monolayered nanodots has potential for tuning of the bandgap energies and achievement of a large ΔE_g.

As well as inorganic materials, graphene and its related structures have been well studied as monolayered carbon materials.[23,24] Monolayered carbon materials are classified into graphene larger than 100 nm in lateral size and nanographene smaller than 100 nm in lateral size. The size and morphology of nanographene were tuned by bottom-up syntheses.[24] Although a variety of inorganic monolayers based on transition metal oxides have been synthesized through exfoliation of the layered compounds, previous works were not fully focused on their lateral size and morphology. Since the precursor layered compounds are typically synthesized by a solid-state reaction at high temperature, the lateral size of the layered materials is in the micrometer scale. The microscopy images showed that the lateral sizes of the monolayered sheets were decreased from those of the pristine layered materials. However, the lateral sizes and morphologies were not fully controlled after exfoliation. The monolayered clusters of molybdenum sulfide, lead iodide, and the related compounds were prepared in earlier works.[25,26] Yoon et al. reported the direct synthesis of a titanate monolayer less than 10 nm in lateral size.[27] The selective syntheses of the monolayered nanodots were not fully studied in transition metal oxides. For syntheses of monolayered nanodots, nanocrystals of layered compounds are required as the precursor materials. We prepared the precursor nanocrystals for exfoliation through aqueous solution processes.[28,29] Our target lateral size of the monolayered nanodots is less than 5 nm.

In the present work, we have synthesized monolayered nanodots of transition metal oxides, such as titanium, tungsten, and manganese oxides. The nanocrystals of the layered compounds less than 10 nm in size were obtained through aqueous solution processes at room temperature.[28,29] The nanostructures can be easily obtained through low-temperature solution processes. The exfoliation of the resultant nanocrystals directed the formation of the monolayered nanodot materials. The remarkable blueshift of the bandgap energy was induced by the formation of the monolayered nanodots.

RESULTS AND DISCUSSION

Monolayer Nanodots of a Titanium Oxide. Nanocrystals of the layered sodium titanate were synthesized through the aqueous solution process reported in our previous work (Figure 2).[28a] An equal volume of the two aqueous solutions each

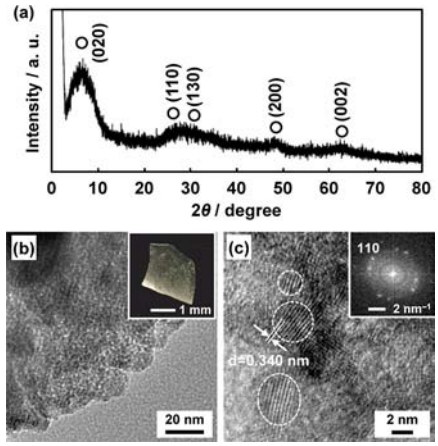

Figure 2. Structure and morphology of the layered sodium titanate nanocrystals: (a) XRD pattern; (b) the macroscopic image of the bulk objects (inset) and FETEM image; (c) HRTEM image and its Fourier transform (inset). The circles in panel a indicate the peak positions of a layered sodium titanate with the lepidocrocite structure.

containing 5 mmol dm^{-3} titanium fluoride (TiF_4) and 50 mmol dm^{-3} sodium hydroxide (NaOH) were mixed at room temperature. After 3 days, the resultant precipitates were collected by centrifugation and then dried at room temperature. The X-ray diffraction (XRD) pattern of the resultant material can be assigned to a layered sodium titanate although the peaks were broadened (Figure 2a).[15c,30] On the basis of Scherrer's equation, the size of the crystallites is estimated to 1.7 nm. The transparent bulk objects approximately 2 mm in size were formed after drying (the inset of Figure 2b). The nanocrystals 2–5 nm in size were observed on the images of field-emission transmission electron microscopy (FETEM) (Figure 2b). On the basis of these results, the macroscopic transparent objects can be regarded as a homogeneous and disordered assembly of the densely packed titanate nanocrystals.[28] The lattice fringes 0.340 nm corresponding to the (110) plane of the titanate were observed on the images of high-resolution transmission electron microscopy (HRTEM) (Figure 2b). The resultant nanocrystals of the layered sodium titanate had a lepidocrocite structure with the chemical formula of $Na_{0.80}Ti_{1.80}\square_{0.2}O_4 \cdot xH_2O$ ($\square$: vacancy, $x < 1.17$).[28a]

dx.doi.org/10.1021/ja400443a | J. Am. Chem. Soc. 2013, 135, 4501–4508

The exfoliation method of the layered titanate compound was referred to in previous works.[15a] The intercalated sodium ions (Na^+) in the layered titanate were exchanged to protons through acid treatment with immersion in hydrochloric acid (HCl). Then, the resultant nanocrystals of the protonated titanate were dispersed in an aqueous solution containing tetrabutlyammonium hydroxide (TBAOH) to promote exfoliation. The resultant colloidal liquid was centrifuged to remove the dispersed pristine nanocrystals without exfoliation. The detailed experimental methods were described in the Supporting Information. The intercalated Na^+ in the interlayer space was exchanged to protons after the acid treatment (Figure S1, Supporting Information). The subsequent TBAOH treatment led to the formation of a white turbid colloidal liquid. After centrifugation, the transparent liquid exhibiting Tyndall light scattering was obtained (inset of Figure 3a). The nanoscale objects 2−5 nm in size were observed on the bright-field FETEM image (Figure 3a). Similar nanostructures were observed on the images of high-angle-annular dark-field scanning transmission electron microscopy (HAADF-STEM) (Figure 3b). The lateral size of the nanoscale objects around 5 nm in size was consistent with that of the pristine layered titanate nanocrystals. The thickness of the nanoscale objects was estimated to 0.77 nm by atomic force microscopy (AFM) (Figure 3c,d). The dispersion liquid of the anionic titanate nanodots was deposited on a silicon (Si) substrate coated with polyethylenimine (PEI) as a cationic polymer. Compared with the PEI-coated Si substrate (Figure 3d), the nanoscale objects with 0.77 nm in thickness were observed on the surface (Figure 3c). The thickness is consistent with that of the micrometer-sized monolayered titanate.[31] These results indicate that the monolayered nanodots of a titanium oxide around 2 nm in the lateral size and 0.77 nm in the thickness were generated in the colloidal liquid.[32]

Figure 3e summarizes the UV−vis spectra and their Tauc plots of the monolayered nanodots and their reference samples. The remarkable blueshift of the absorption edges was observed on the monolayered nanodots (spectrum iv in Figure 3e). While the E_g value of the micrometer-sized titanate crystals was 3.24 eV (spectrum i in Figure 3e), the E_g value of the pristine layered titanate nanocrystals was estimated to 3.42 eV (spectrum ii in Figure 3e). The blueshift of the E_g value, namely, ΔE_g = 0.18 eV, is ascribed to the quantum size effect. After exfoliation, the E_g value of the monolayered nanodot was widened to 3.90 eV while the E_g value of the micrometer-sized monolayer was 3.84 eV (spectra iii and iv in Figure 3e). The light absorption of TBAOH was not overlapped with that of the monolayered nanodots (Figure S2, Supporting Information). Although the lateral sizes of the monolayered nanodots included some deviations, the UV−vis spectra of the different three batches showed similar absorption behavior (Figure S2, Supporting Information). Compared to these results, the monolayered nanodot induces the larger ΔE_g value based on the stronger quantum size effect. The ΔE_g value of the monolayered nanodots, namely, ΔE_g = 0.76 eV to a bulk anatase, is consistent with the calculation studies as shown in Figure 1a.[33] If the same E_g value is derived by the quantum size effect on an anatase TiO_2 nanoparticle, the diameter needs to be smaller than 0.98 nm. The fact suggests that the strategy for preparation of monolayered nanodots has the potential to achieve the large ΔE_g value.

Synthesis of Tungsten Oxide Monolayer Nanodots. The target material was changed to a tungsten oxide related material to achieve the more remarkable ΔE_g value. Nanocrystals of a layered cesium tungstate were synthesized through an aqueous solution process at room temperature. A layered tungstate has a crystal structure of hexagonal tungsten bronze (HTB) with the tunnel structure consisting of corner-shared $\{WO_6\}$ octahedrons. In the present work, we modified the hydrothermal syntheses of the layered tungstate salts with HTB structure for the aqueous solution syntheses.[35] An aqueous solution containing 20 mmol dm^{-3} sodium tungstate dihydrate ($Na_2WO_4{\cdot}2H_2O$) and 10 mmol dm^{-3} cesium carbonate (Cs_2CO_3), typically 100 cm^3, was mixed with an equal volume of 100 mmol dm^{-3} HCl at room temperature. After a day, the resultant precipitates were collected by centrifugation and then dried at room temperature. The pH of the aqueous solution

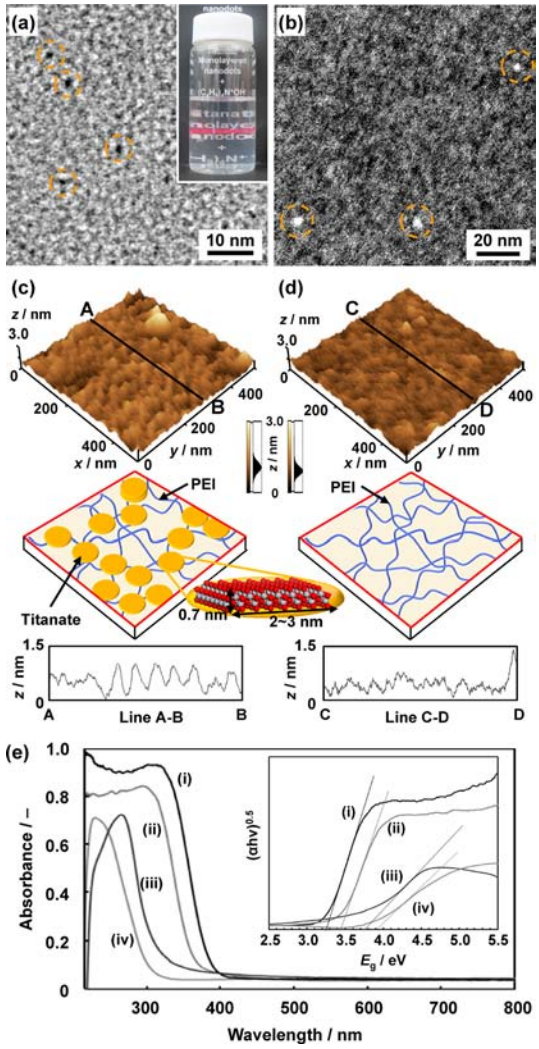

Figure 3. Structure and morphology of the titanium oxide monolayered nanodots: (a) bright-field FETEM image of the monolayered nanodots and a picture of its dispersion liquid exhibiting Tyndall light scattering (inset); (b) HAADF-STEM image (white objects on black background); (c, d) AFM images of the titanate monolayered nanodots on the PEI-coated substrate (c) and the PEI-coated substrate as the reference (d) with the distribution of the height, the schematic illustrations (middle), and the height profiles on the lines A−B and C−D (lower) 500 nm in the length scales corresponding to the respective images;[34] (e) UV−vis spectra and their corresponding Tauc plots (inset) of the bulk titanate crystal (i), the precursor titanate nanocrystal (ii), the micrometer-sized monolayer (iii), and the monolayered nanodot (iv).

dx.doi.org/10.1021/ja400443a | J. Am. Chem. Soc. 2013, 135, 4501−4508

containing tungstate source was adjusted to 1.3−3.2 for the selective synthesis of the HTB structure. Cesium ion (Cs^+) was added to direct the formation of the cesium salt and the tunnel-type crystal structure.[36] All the peaks on the XRD pattern were assigned to those of a layered cesium tungstate ($Cs_4W_{11}O_{35}$) with the HTB structure (Figure 4a).[37] Since the peaks were

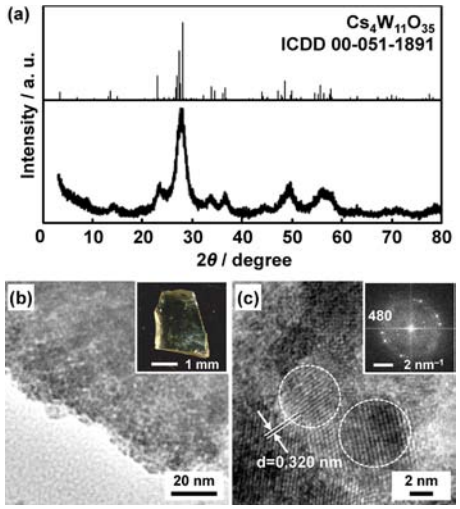

Figure 4. Structure and morphology of the layered cesium tungstate nanocrystals: (a) XRD pattern with the peak positions in the ICDD card; (b) the macroscopic image of the bulk objects (inset) and FETEM image; (c) HRTEM image and its Fourier transform (inset).

broadened, further assignment was carried out after thermal treatment at 800 °C for 5 h in air (Figure S3, Supporting Information). The chemical formula of the layered cesium tungstate was determined as $A_{1.2}Cs_{2.8}W_{11}O_{35}{\cdot}yH_2O$ (A = Na^+ and H^+, y < 10.5) by energy-dispersive X-ray (EDX) and thermogravimetric (TG) analyses (Figure S4, Supporting Information). Transparent bulk objects 2−5 mm in size were obtained (the inset of Figure 4b). The nanocrystals of the tungstate less than 5 nm in size were observed on the FETEM images (Figure 4b). These results suggest that the densely packed nanocrystals formed the homogeneous and disordered assembly.[28] The nanocrystals with the lattice fringes of 0.320 nm corresponding to the (480) plane of the tungstate were observed on the HRTEM image (Figure 4c). The formation of the nanocrystals and their specific assembly was the same as those of the titanate nanocrystals.

The delamination method of the layered tungstate was referred to in a previous work.[15h] The interlayer cations such as Na^+ and Cs^+ were exchanged to protons through acid treatment with HCl. Then, the protonated tungstate nanocrystals were dispersed in an aqueous solution of TBAOH to promote exfoliation. On the basis of EDX and TG analyses, the chemical formula of the protonated layered tungstate was estimated to $H_{2.6}Cs_{1.4}W_{11}O_{35}{\cdot}yH_2O$ (y < 9.2) (Figure S4, Supporting Information). In the crystal structure of $Cs_4W_{11}O_{35}$, 25 mol % of Cs^+ is intercalated in the interlayer space. The other 75 mol % of Cs^+ occupies the inside of the hexagonal tunnel structure on each layer consisting of the $\{WO_6\}$ octahedrons. The intercalated Cs^+ in the interlayer space is preferentially exchanged to protons by acid treatment. Since about 65 mol % of Cs^+ in $Cs_4W_{11}O_{35}$ was exchanged to a proton in the resultant $H_{2.6}Cs_{1.4}W_{11}O_{35}{\cdot}yH_2O$ (y < 9.2), the exchange of the interlayer Cs^+ to protons was achieved in the present study. Then, the protonated tungstate nanocrystals were dispersed in an aqueous solution of tetrabutlyammonium hydroxide (TBAOH) to promote exfoliation. The transparent colloidal liquid exhibiting Tyndall light scattering was obtained after TBAOH treatment and subsequent centrifugation (the inset of Figure 5a). The

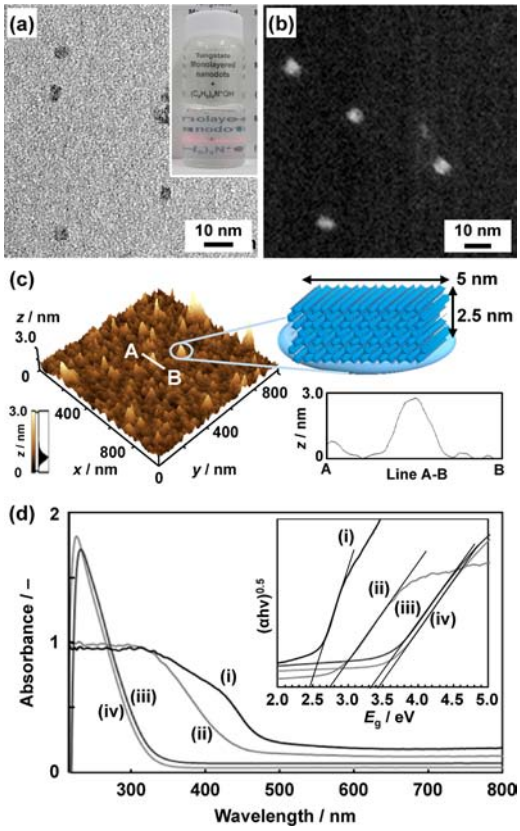

Figure 5. Structure and morphology of the tungsten oxide monolayered nanodots: (a) bright-field FETEM image of the monolayered nanodots and a picture of its dispersion liquid exhibiting Tyndall light scattering (inset); (b) HAADF-STEM image; (c) AFM image with the distribution of the height, the height profile on the line A−B 180 nm in the length scale corresponding to the image,[34] and the schematic illustration with the crystal structure of the tungstate; (e) UV−vis spectra and their corresponding Tauc plots (inset) of the bulk tungstate crystal (i), the precursor tungstate nanocrystal (ii), the micrometer-sized monolayer (iii), and the monolayered nanodot (iv).

nanoscale objects about 5 nm in size were observed on the bright-field FETEM and HAADF-STEM images (Figure 5a,b). The lateral size was not changed after TBAOH treatment. The thickness of the nanoscale objects was estimated to 2.66 nm by AFM observations (Figure 5c). The thickness is consistent with that of the micrometer-sized monolayered tungstate.[15h] These results indicate the formation of the tungstate monolayered nanodots 5 nm in lateral size and 2.5 nm in thickness in the colloidal liquid.

Figure 5d summarizes the UV−vis spectra and their Tauc plots of the monolayered nanodots and their reference samples. The monolayered nanodots of the tungstate showed a remarkable blueshift of the bandgap energy, namely, ΔE_g = 1.00 eV, compared to the bulk material. The E_g value of the precursor layered tungstate nanocrystals was estimated to 2.77 eV (curve ii in Figure 5d). After exfoliation, the E_g value was shifted to 3.46 eV on the monolayered nanodots (curve iv in Figure 5d). The bulk structure of the precursor layered

dx.doi.org/10.1021/ja400443a | J. Am. Chem. Soc. 2013, 135, 4501−4508

tungstate as a reference was prepared by the calcination of the nanocrystals (Figure S5, Supporting Information). The bulk layered tungstate and its exfoliated monolayer showed E_g = 2.46 eV and E_g = 3.35 eV (curves i and iii in Figure 5d), respectively. On the basis of these results, the ΔE_g value for the formation of the monolayered nanodots was estimated to be 1.00 eV compared to the bulk material. Since tungsten oxides and tungstate salts have a number of crystal structures, the reduced effective mass of a certain crystal phase is not precisely studied in previous works. Herein, we estimated the reduced effective masses such as μ_{xy} and μ_z based on eq 1 by using the reference bulk sample. The large ΔE_g value of the monolayered nanodots can be explained by the calculated values of the effective masses. The exfoliation of the bulk layered tungstate showed ΔE_g = 0.89 eV (curves i and iii in Figure 5d). The ΔE_g value is mainly ascribed to the decrease in the thickness with exfoliation. Since the smaller first term in eq 1 related to the lateral size can be ignored, the μ_z value is calculated to be $0.068m_e$ by using the second term of eq 1. The formation of the precursor layered tungstate nanocrystals 5 nm in size showed ΔE_g = 0.31 eV compared to the bulk layered tungstate (curves i and ii in Figure 5d). The μ_z value is assumed to be $0.068m_e$ for the nanocrystals 5 nm in size. The μ_{xy} value can be calculated to be $0.33m_e$ on the assumption of the cubic shape 5 nm in size. On the basis of these μ_{xy} and μ_z values, the ΔE_g value for generation of the monolayered nanodots 5 nm in lateral size and 2.5 nm in thickness can be calculated to be 0.98 eV by using eq 1. The calculated ΔE_g value is consistent with the experimental results. Compared to the results of the titanium oxide monolayered nanodots, the smaller μ_{xy} value led to the large ΔE_g value by the formation of the monolayered nanodots. There results imply that generation of the monolayered nanodots has the potential for the tuning of properties based on size effects.

Monolayer Nanodots of a Manganese Oxide. Nanocrystals of birnessite-type sodium manganate were synthesized through the aqueous solution process by the modified method in our previous work (Figure 6).[29] The aqueous solution containing 20 mmol dm^{-3} manganese chloride tetrahydrate ($MnCl_2{\cdot}4H_2O$), 10 mmol dm^{-3} poly(acrylic acid) (PAA, M_r = 2×10^3), and 1.13 mol dm^{-3} hydrogen peroxide (H_2O_2) was mixed with an equal volume of 200 mmol dm^{-3} NaOH aqueous solution at room temperature. In the synthetic process, PAA and H_2O_2 played important roles for the control of the morphologies and the oxidation states, respectively.[29] The XRD pattern was assigned to that of a birnessite-type sodium manganate with a layered structure (Figure 6a).[29b] On the basis of the TG analysis and the titration experiment, the chemical formula of the resultant manganese oxide nanocrystals was determined as $Na_{0.44}MnO_2{\cdot}zH_2O$ ($z < 0.71$). The size of the crystallite was estimated to be 5.6 nm by Scherrer's equation on the peak of the (110) plane. The sheetlike morphologies consisting of the nanocrystals less than 10 nm in size were observed on the FESEM and FETEM images (Figure 6b,c). The HRTEM image shows the lattice fringe of 0.248 nm corresponding to the (100) plane (Figure 6d).

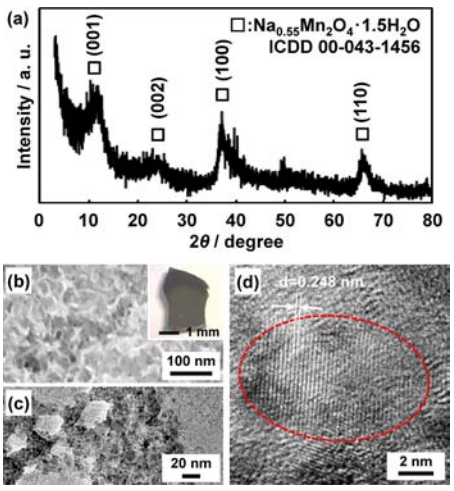

Figure 6. Structure and morphology of the sodium manganate nanocrystals: (a) XRD pattern; (b) the macroscopic image of the bulk objects (inset) and FESEM image; (c) FETEM image; (d) HRTEM image. The squares in panel a indicate the peak positions of a birnessite-type sodium manganese oxide in the ICDD card.

The delamination method of a birnessite-type manganate was referred to in a previous work.[15d] The intercalated Na^+ was exchanged to a proton and then tetramethylammonium hydroxide (TMAOH). The resultant tetramethylammonium cation (TMA^+)-intercalated compound was dispersed in a TBAOH aqueous solution to promote delamination. After HCl treatment, the intercalated Na^+ was exchanged to a proton (Figure S6, Supporting Information). The chemical formula of the protonated manganese oxide was determined as $H_{0.33}MnO_2{\cdot}0.85H_2O$. The TMA^+-intercalated compound was prepared to expand the interlayer space prior to immersion in a TBAOH aqueous solution (Figure S7, Supporting Information). After TBAOH treatment, the transparent brown colloid was obtained (the inset of Figure 7a). The nanoscale objects around 10 nm in lateral size were observed on the bright-field FETEM and HAADF-STEM images (Figure 7a,b). These lateral sizes of the nanoscale objects were consistent with those of the precursor manganate nanocrystals before exfoliation. The average thickness of the nanoscale objects was estimated to be 0.69 nm by AFM measurements (Figure 7c). The thickness is consistent with that of the micrometer-sized manganese oxide monolayers including the surface hydrated layer in a previous paper.[15d] These results suggest that the monolayered nanodots of manganese oxide were synthesized from the precursor nanocrystals.

The resultant monolayered nanodots of manganese oxide showed broadened absorption around 380 nm on the UV−vis spectrum of the dispersion liquid (Figure 7d). In contrast, the precursor manganese oxide before the exfoliation showed the absorption over the entire range from UV to visible light on the diffuse reflectance spectrum. It was reported that the nanometer-sized and monolayered manganese oxides have similar broadened absorption around 380 nm.[15d,38] The absorption originates from the electron transition between the 3d orbitals of the $\{MnO_6\}$ octahedron in manganese oxides with nanometer size. Although the formation of the monolayered materials in the present study was supported by the appearance of absorption around 380 nm, the peak position was not changed by the formation of the monolayered nanodots. The absorption coefficient (ε) was calculated to be $\varepsilon = 1.17 \times 10^4$ cm^{-1} dm^3 mol^{-1} at 380 nm on the resultant monolayered nanodots. In previous work, the micrometer-sized monolayers of manganese oxide showed the ε values ranging from 8.5×10^3 to 1.13×10^4 cm^{-1} dm^3 mol^{-1}.[15c,39] Since the birnessite-type manganate is not a semiconductor material, the absorption

dx.doi.org/10.1021/ja400443a | J. Am. Chem. Soc. 2013, 135, 4501−4508

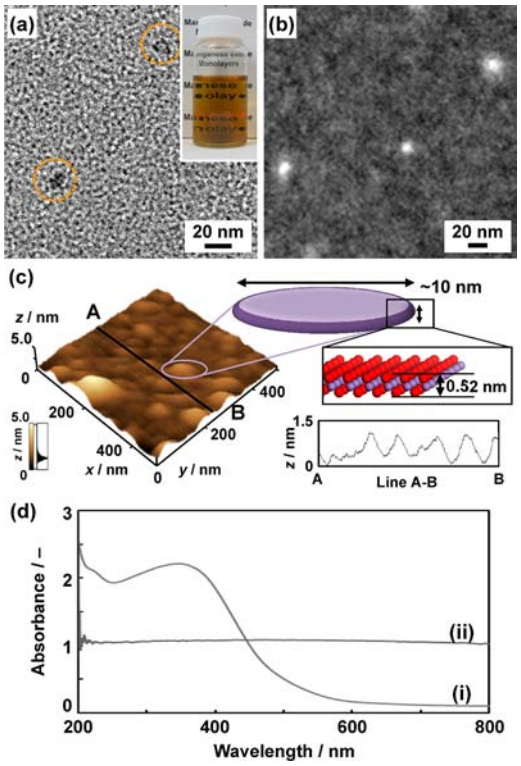

Figure 7. Structure and morphology of the manganese oxide monolayered nanodots: (a) bright-field FETEM image of the monolayered nanodots and a picture of its dispersion liquid exhibiting Tyndall light scattering (inset); (b) HAADF-STEM image; (c) AFM image with the distribution of the height, the height profiles on the line A–B 500 nm in the length scale corresponding to the image,[34] and the schematic model of the monolayered nanodot consisting of birnessite-type manganese oxide; (d) UV–vis spectra of the monolayered nanodots in the dispersion liquid (i) and diffuse reflectance spectra of the precursor manganese oxide nanocrystals (ii).

behavior, such as the peak position and the ε value of the absorption, would not be influenced by the lateral size.

Formation Processes and Properties of the Monolayered Nanodots. The precursor nanocrystals of the layered compounds less than 10 nm in size were synthesized through aqueous solution processes at room temperature. In general, it is not so easy to prepare the nanocrystals of layered compounds with a homogeneous size by typical synthetic methods. The precursor layered compounds were synthesized by a solid-state reaction at high temperature. The nanocrystals with the tuned size are not easily obtained because of the grain growth by sintering. In solution syntheses, layered compounds easily form the anisotropic sheetlike morphologies originating from the crystal structures. Synthesis of the nanocrystals requires morphology control with growth inhibition in the lateral direction of the sheet. Some previous works have showed the syntheses of the layered compounds less than 100 nm in lateral size.[40] In the present study, the nanocrystals of the layered compounds were obtained in homogeneous and disordered assemblies. The formation of the nanocrystals and their characteristic assembly states is induced by the aqueous solution syntheses under the high supersaturated conditions near the isoelectric point or the point of zero charge.[28a] At the initial stage, a large number of nuclei are generated under the high supersaturated conditions after the mixing of the two precursor solutions. The crystal phases are determined by the solution conditions, such as pH and concentration of the precursor solutions. The hydrated surface is formed on the resultant nanocrystals near the isoelectric point or the point of zero charge.[28a] Further growth of the nanocrystals including the formation of the 2D morphologies are inhibited by the surface hydration. Therefore, the homogeneous dispersion of the nanocrystals is achieved in an aqueous medium. The homogeneous and disordered assemblies of the nanocrystals were generated without formation of secondary particles through the aggregation. The bulk objects were eventually obtained after drying, as shown in the insets of Figures 2b, 4b, and 6b. In this way, the nanocrystals of the layered compounds are synthesized in homogeneous and disordered assemblies. If the synthesis and growth conditions, such as the concentrations, temperature, and incubation time, are tuned in the solution process, the lateral size of the precursor nanocrystals and its distribution can be controlled. The addition of surface capping agents is also effective for fine-tuning of the lateral size. However, further studies are required for the fine-tuning of the size and its distribution in the solution processes under mild conditions in the present state. The synthetic approach has potential for application to other transition metal oxides with layered structure.

It is inferred that the hydrated nanocrystals is favorable for the dispersion and the subsequent exfoliation in aqueous media. In the present work, the sizes of the monolayered nanodots were not changed from those of the precursor nanocrystals after the exfoliation. In contrast, previous studies have showed that the lateral sizes of micrometer-scale layered compounds are not always kept on the monolayered structures after exfoliation. The monolayered structures are broken into the smaller flakes through the introduction of bulky organic cations and the subsequent exfoliation processes. Since bulky organic cations are not smoothly introduced in the interlayer space of the micrometer-scale layered compounds, exfoliated fragments would be formed. In the current study, water-dispersible nanocrystals facilitate the smooth introduction of the organic cations and the subsequent exfoliation in aqueous media. Therefore, the monolayered nanodots were obtained from the precursor nanocrystals without changes of the lateral size.

The present work suggests that generation of monolayered nanodots expands the tuning range of the bandgap energies in semiconductor materials. The monolayered nanodots of titanium and tungsten oxides showed ΔE_g = 0.76 eV and ΔE_g = 1.00 eV compared to the bulk materials of these compounds, respectively. Since the absorption of manganese oxide results from the electron transition of the 3d orbitals, the absorption behavior, such as the peak position and absorption coefficient, is not influenced by the decrease in the lateral size of the monolayered compounds. ΔE_g = 0.76 eV for titanium oxide and ΔE_g = 1.00 eV for tungsten oxide are consistent with those calculated by eq 1. As represented on the model calculations in Figure 1, the large ΔE_g value can be obtained by the decrease in the lateral size of the ultrathin nanomaterial. Furthermore, the reduced effective mass and its anisotropy, such as μ_{xy} and μ_z, remarkably influence the ΔE_g value of the monolayered nanodots. These results and calculations suggest that generation of the ultrathin tiny objects has the potential for tuning the bandgap energies. The strategy to form ultrathin tiny structures can be applied to not only the layered compounds but also the other semiconductor materials for tuning of the bandgap energies.

dx.doi.org/10.1021/ja400443a | J. Am. Chem. Soc. 2013, 135, 4501–4508

CONCLUSIONS

The monolayered nanodots of transition metal oxides, such as titanium, tungsten, and manganese oxides, have been prepared through the exfoliation of precursor nanocrystals. The nanocrystals of the layered compounds less than 10 nm in lateral size were formed in homogeneous and disordered assemblies by syntheses in an aqueous solution at room temperature. The exfoliation of the nanocrystals led to generation of the monolayered structures without changes of the lateral size. The resultant monolayered nanodots of titanium and tungsten oxides exhibited a remarkable blueshift of the bandgap energies, namely, ΔE_g = 0.76 eV and ΔE_g = 1.00 eV, respectively. The calculations based on eq 1 supported the experimental results. The present approaches for morphological control and tuning of the properties can be applied to a variety of nanomaterials. Monolayered nanodots have the potential for a building block of composites in a molecular level and for a variety of applications.

ASSOCIATED CONTENT

Supporting Information

Experimental procedures; calculation processes of the ΔE_g values of monolayered nanodots; and additional data supported by XRD patterns, EDX and TG analyses, UV−vis spectra, and FESEM images. This material is available free of charge via the Internet at http://pubs.acs.org.

AUTHOR INFORMATION

Corresponding Author

oakiyuya@applc.keio.ac.jp; hiroaki@applc.keio.ac.jp

Notes

The authors declare no competing financial interest.

ACKNOWLEDGMENTS

This work was partially supported by Grant-in-Aid for Scientific Research (no. 22107010) on Innovative Areas of "Fusion Materials: Creative Development of Materials and Exploration of Their Function through Molecular Control" (no. 2206) (H.I.) from the Ministry of Education, Culture, Sports, Science and Technology and for Young Scientist (A, no. 22685022) (Y.O.) and Challenging Exploratory Research (no. 24655199) (Y.O.) from Japan Society of the Promotion of Science.

REFERENCES

(1) (a) Yin, Y.; Alivisatos, A. P. *Nature* **2005**, *473*, 664. (b) Wang, D.; Lieber, C. M. *Nat. Mater.* **2003**, *2*, 356. (c) Xia, Y.; Xiong, Y.; Lim, B.; Skrabalak, S. E. *Angew. Chem., Int. Ed.* **2009**, *48*, 60. (d) Tian, B.; Kempa, T. J.; Lieber, C. M. *Chem. Soc. Rev.* **2009**, *38*, 16. (e) Tao, A. R.; Habas, S.; Yang, P. *Small* **2008**, *3*, 310. (f) Antonietti, M.; Ozin, G. A. *Chem.—Eur. J.* **2004**, *10*, 28. (g) Grinthal, A.; Kang, S. H.; Epsteina, A. K.; Aizenberg, M.; Khan, M.; Aizenberg, J. *Nano Today* **2011**, *7*, 35. (h) Liu, J. W.; Liang, H. W.; Yu, S. H. *Chem. Rev.* **2012**, *112*, 4770. (i) Gough, D. V.; Juhl, A. T.; Braun, P. V. *Mater. Today* **2009**, *12*, 28.

(2) (a) Park, J.; Joo, J.; Kwon, S. C.; Jang, Y.; Hyeon, T. *Angew. Chem., Int. Ed.* **2007**, *46*, 4630. (b) Pinna, N.; Niederberger, M. *Angew. Chem., Int. Ed.* **2008**, *47*, 5292. (c) Murray, C. B.; Kagan, C. R.; Bawendi, M. G. *Annu. Rev. Mater. Sci.* **2000**, *30*, 545. (d) Talapin, D. V.; Lee, J.-S.; Kovalenko, M. V.; Shevchenko, E. V. *Chem. Rev.* **2010**, *110*, 389. (e) Cademartiri, L.; Ghadimi, A.; Ozin, G. A. *Acc. Chem. Res.* **2008**, *41*, 1820. (f) Zeng, H. C. *J. Mater. Chem.* **2011**, *21*, 7511.

(3) (a) Cölfen, H.; Mann, S. *Angew. Chem., Int. Ed.* **2003**, *42*, 2350. (b) Cölfen, H.; Antonietti, M. *Angew. Chem., Int. Ed.* **2005**, *44*, 5576. (c) Zhou, L.; O'Brien, P. *Small* **2008**, *4*, 1566. (d) Song, R. Q.; Cölfen, H. *Adv. Mater.* **2010**, *22*, 1301.

(4) (a) Yokoi, T.; Sakamoto, Y.; Terasaki, O.; Kubota, Y.; Okubo, T.; Tatsumi, T. *J. Am. Chem. Soc.* **2006**, *128*, 13664. (b) Fukao, M.; Sugawara, A.; Shimojima, A.; Fan, W.; Arunagirinathan, M. A.; Tsapatsis, M.; Okubo, T. *J. Am. Chem. Soc.* **2009**, *131*, 16344.

(5) Zarzar, L. D.; Swartzentruber, B. S.; Harper, J. C.; Dunphy, D. R.; Aizenberg, J.; Kaehr, B. *J. Am. Chem. Soc.* **2012**, *134*, 4007.

(6) (a) Oaki, Y.; Imai, H. *Angew. Chem., Int. Ed.* **2005**, *44*, 6571. (b) Oaki, Y.; Imai, H. *Small* **2006**, *2*, 66. (c) Oaki, Y.; Kotachi, A.; Miura, T.; Imai, H. *Adv. Funct. Mater.* **2006**, *16*, 1633.

(7) Li, M.; Schnablegger, H.; Mann, S. *Nature* **1999**, *402*, 393.

(8) Polleux, J.; Pinna, N.; Antonietti, M.; Niederberger, M. *J. Am. Chem. Soc.* **2005**, *127*, 15595.

(9) Shevchenko, E. V.; Talapin, D. V.; Kotov, N. A.; O'Brien, S.; Murray, C. B. *Nature* **2006**, *439*, 55.

(10) Oaki, Y.; Kajiyama, S.; Nishimura, T.; Imai, H.; Kato, T. *Adv. Mater.* **2008**, *20*, 3633.

(11) Yao, K. X.; Yin, X. M.; Wang, T. H.; Zeng, H. C. *J. Am. Chem. Soc.* **2010**, *132*, 6131.

(12) Huo, Z.; Tsung, C.-K.; Huang, W.; Fardy, M.; Yan, R.; Zhang, X.; Li, Y.; Yang, P. *Nano Lett.* **2009**, *9*, 1260.

(13) (a) Schaak, R. E.; Mallouk, T. E. *Chem. Mater.* **2002**, *14*, 1455. (b) Sasaki, T. *J. Ceram. Soc. Jpn.* **2007**, *115*, 9. (c) Osada, M.; Sasaki, T. *J. Mater. Chem.* **2009**, *19*, 2503. (d) Ma, R.; Sasaki, T. *Adv. Mater.* **2010**, *22*, 5082. (e) Wang, Q.; O'Hare, D. *Chem. Rev.* **2012**, *112*, 4124. (f) Okamoto, H.; Sugiyama, Y.; Nakano, H. *Chem.—Eur. J.* **2011**, *17*, 9864. (g) Nakato, T.; Miyamoto, N. *Materials* **2009**, *2*, 1734.

(14) (a) Lerf, A.; Schöllhorn, R. *Inorg. Chem.* **1977**, *16*, 2950. (b) Clement, R.; Garnier, O.; Jegoudez, J. *Inorg. Chem.* **1986**, *25*, 1404. (c) Nazar, L. F.; Jacobson, A. J. *J. Chem. Soc. Chem. Commun.* **1986**, 570. (d) Joensen, P.; Frindt, R. F.; Morrison, S. R. *Mater. Res. Bull.* **1986**, *21*, 457. (e) Treacy, M. M. J.; Rice, S. B.; Jacobson, A. J.; Lewandowski, J. T. *Chem. Mater.* **1990**, *2*, 279. (f) Domen, K.; Ebina, Y.; Ikeda, S.; Tanaka, A.; Kondo, J. N.; Maruya, K. *Catal. Today* **1996**, *28*, 167. (g) Schaak, R. E.; Mallouk, T. E. *Chem. Mater.* **2000**, *12*, 3427. (h) Adachi-Pagano, M.; Forano, C.; Besse, J. P. *Chem. Commun.* **2000**, 91. (i) Hibino, T.; Willam, J. *J. Mater. Chem.* **2001**, *11*, 1321. (j) Yamamoto, N.; Okuhara, T.; Nakato, T. *J. Mater. Chem.* **2001**, *11*, 1858.

(15) (a) Sasaki, T.; Watanabe, M.; Hashizume, H.; Yamada, H.; Nakazawa, H. *J. Am. Chem. Soc.* **1996**, *118*, 8329. (b) Sasaki, T.; Watanabe. *J. Am. Chem. Soc.* **1998**, *120*, 4682. (c) Sasaki, T.; Kooli, F.; Iida, M.; Michiue, Y.; Takenouchi, S.; Yajima, Y.; Izumi, F.; Chakoumakos, B. C.; Watanabe, M. *Chem. Mater.* **1998**, *10*, 4123. (d) Omomo, Y.; Sasaki, T.; Watanabe, M.; Wang, L. *J. Am. Chem. Soc.* **2003**, *125*, 3568. (e) Sakai, N.; Ebina, Y.; Takada, K.; Sasaki, T. *J. Am. Chem. Soc.* **2004**, *126*, 5851. (f) Liu, Z.; Ma, R.; Ebina, Y.; Takada, K.; Sasaki, T. *Chem. Mater.* **2007**, *19*, 6504. (g) Fukuda, K.; Akatsuka, K.; Ebina, Y.; Ma, R.; Takada, K.; Nakai, I.; Sasaki, T. *ACS Nano* **2008**, *2*, 1689. (h) Fukuda, K.; Akatsuka, K.; Ebina; Osada, M.; Sugimoto, W.; Kimura, M.; Sasaki, T. *Inorg. Chem.* **2012**, *51*, 1540.

(16) Haraguchi, K.; Takehisa, T. *Adv. Mater.* **2002**, *14*, 1120.

(17) Nakano, H.; Mitsuoka, T.; Harada, M.; Horibuchi, K.; Nozaki, H.; Takahashi, N.; Nonaka, T.; Seno, Y.; Nakamura, H. *Angew. Chem., Int. Ed.* **2006**, *45*, 6303.

(18) Takahashi, N.; Hata, H.; Kuroda, K. *Chem. Mater.* **2011**, *23*, 266.

(19) Sandroff, C. J.; Hwang, D. M.; Chung, W. M. *Phys. Rev. B* **1986**, *33*, 5953 (The small terms were ignored in the calculation.).

(20) (a) Kormann, C.; Bahnemann, D. W.; Hoffmann, M. R. *J. Phys. Chem.* **1988**, *92*, 5169. (b) Satoh, N.; Nakahima, T.; Kamikura, K.; Yamamoto, K. *Nat. Nanotechnol.* **2008**, *3*, 106.

(21) The detailed calculation processes were described in the Supporting Information.

(22) Lamberti, C. *Microporous Mesoporous Mater.* **1999**, *30*, 155 (The quantum wire confined in the titanosilicate microporous compound showed the bandgap energy 4.03 eV with ΔE_g = 0.83 eV. However, the quantum wire is embedded in the molecular sieve consisting of silica. The wire was not extracted from the molecular sieve.).

(23) (a) Novoselov, K. S.; Geim, A. K.; Morozov, S. V.; Jiang, D.; Zhang, Y.; Dubonos, S. V.; Grigorieva, I. V.; Firsov, A. A. *Science* **2004**, *306*, 666. (b) Novoselov, K. S. *Angew. Chem., Int. Ed.* **2011**, *50*, 6986.
(24) Chen, L.; Hernandez, Y.; Feng, X.; Müllen, K. *Angew. Chem., Int. Ed.* **2012**, *51*, 7640.
(25) (a) Micic, O. I.; Zongguan, L.; Mills, G.; Sullivan, J. C.; Meisel, D. *J. Phys. Chem.* **1987**, *91*, 6221. (b) Sandroff, C. J.; Kelty, S. P.; Hwang, D. M. *J. Chem. Phys.* **1986**, *85*, 5337.
(26) Peterson, M. W.; Nenadovic, M. T.; Rajh, T.; Herak, R.; Micic, O. I.; Goral, J. P.; Nozik, A. J. *J. Phys. Chem.* **1988**, *92*, 1400.
(27) Tae, E. L.; Lee, K. E.; Jeong, J. S.; Yoon, K. B. *J. Am. Chem. Soc.* **2008**, *130*, 6534.
(28) (a) Oaki, Y.; Nakamura, K.; Imai, H. *Chem.—Eur. J.* **2012**, *18*, 2825. (b) Oaki, Y.; Anzai, T.; Imai, H. *Adv. Funct. Mater.* **2010**, *20*, 4127.
(29) (a) Oaki, Y.; Imai, H. *J. Mater. Chem.* **2007**, *17*, 316. (b) Oaki, Y.; Imai, H. *Angew. Chem., Int. Ed.* **2007**, *46*, 4951. (c) Oba, M.; Oaki, Y.; Imai, H. *Adv. Funct. Mater.* **2010**, *20*, 4279.
(30) Takezawa, Y.; Imai, H. *Small* **2006**, *2*, 390.
(31) Sasaki, T.; Watanabe, M. *J. Phys. Chem. B* **1997**, *101*, 10159.
(32) We tried to characterize the crystal structure of the monolayered nanodots after exfoliation by using a wide-angle XRD. The XRD measurement was performed on the monolayered nanodots of the titanate coated on the substrate. In this case, however, the peaks were not detected on the XRD pattern. The specimen was changed to a small amount of the wet paste obtained after the centrifugation of the dispersion liquid. The peaks were not observed on the XRD pattern of the paste. In the TEM observations, HRTEM images and SAED patterns regarding the crystalline structure of the monolayered nanodots were not acquired at present. Therefore, we used the term not monolayered nanocrystal but monolayered nanodot in the present work.
(33) The L_x and L_y values were assumed to be $L_x = L_y = 2R$, where $2R$ is the observed approximate diameter of the precursor nanocrystals before exfoliation. Therefore, the calculation of ΔE_g included some deviation. In a precise sense, the anisotropy of the size, the size distribution, and the effective mass, such as μ_x and μ_y values, should be considered for the calculation.
(34) The lateral length scale of the AFM observation generally depends on the curvature factor of a cantilever originating from the factory-default value and the deterioration with use. Therefore, we concluded that the correct lateral sizes of the monolayered nanodots were not estimated from the AFM observations. In the present study, the thickness and the lateral size were estimated from the AFM observation and the TEM images, respectively.
(35) (a) Guo, J.; Reis, K. P.; Whittingham, M. S. *Solid State Ionics.* **1992**, *53*, 305. (b) Reis, K. P.; Ramanan, A.; Whittingham, M. S. *Chem. Mater.* **1990**, *2*, 219.
(36) Kudo, T.; Oi, J.; Kishimoto, A.; Hiratani, M. *Mater. Res. Bull.* **1991**, *26*, 779.
(37) Solodovnicov, S. F.; Ivannikova, N. V.; Solodovnikova, Z. A.; Zolotova, E. S. *Inorg. Mater.* **1998**, *34*, 845.
(38) Gao, Q.; Giraldo, O.; Tong, W.; Suib, S. L. *Chem. Mater.* **2001**, *13*, 778.
(39) Kai, K.; Yoshida, Y.; Kageyama, H.; Saito, G.; Ishigaki, T.; Furukawa, Y.; Kawamata, J. *J. Am. Chem. Soc.* **2008**, *130*, 15938.
(40) (a) Hu, G.; O'Hare, D. *J. Am. Chem. Soc.* **2005**, *127*, 17808. (b) Williams, G. R.; O'Hare, D. *J. Mater. Chem.* **2006**, *16*, 3065. (c) Dinh, C. T.; Seo, Y.; Nguyen, T. D.; Kleitz, F.; Do, T. O. *Angew. Chem., Int. Ed.* **2012**, *51*, 6608.